Biological Psychiatry: CNNI

Archival Report

Parsing Autism Heterogeneity: Transcriptomic Subgrouping of Imaging-Derived Phenotypes in Autism

Johanna Leyhausen, Caroline Gurr, Lisa M. Berg, Hanna Seelemeyer, Bassem Hermila, Tim Schäfer, Andreas G. Chiocchetti, Charlotte M. Pretzsch, Eva Loth, Bethany Oakley, Jan K. Buitelaar, Christian F. Beckmann, Tony Charman, Thomas Bourgeron, Eli Barthome, Tobias Banaschewski, Emily J.H. Jones, on behalf of the EU-AIMS LEAP Group, Declan Murphy, and Christine Ecker

ABSTRACT

BACKGROUND: Neurodevelopmental conditions, such as autism, are highly heterogeneous at both the mechanistic and phenotypic levels. Therefore, parsing heterogeneity is vital for uncovering underlying processes that could inform the development of targeted, personalized support. We aimed to parse heterogeneity in autism by identifying subgroups that converge at both the phenotypic and molecular levels.

METHODS: An imaging transcriptomics approach was used to link neuroanatomical imaging-derived phenotypes in autism to whole-brain gene expression signatures provided by the Allen Human Brain Atlas. Neuroimaging and clinical data of 359 autistic participants ages 6 to 30 years were provided by EU-AIMS (European Autism Interventions) LEAP (Longitudinal European Autism Project). Individuals were stratified using data-driven clustering techniques based on the correlation between brain phenotypes and transcriptomic profiles. The resulting subgroups were characterized on the clinical, neuroanatomical, and molecular levels.

RESULTS: We identified 3 subgroups of autistic individuals based on the correlation between imaging-derived phenotypes and transcriptomic profiles that showed different clinical phenotypes. The individuals with the strongest transcriptomic associations with imaging-derived phenotypes showed the lowest level of symptom severity. The gene sets most characteristic for each subgroup were significantly enriched for genes previously implicated in autism etiology, including processes such as synaptic transmission and neuronal communication, and mapped onto different gene ontology categories.

CONCLUSIONS: Autistic individuals can be subgrouped based on the transcriptomic signatures associated with their neuroanatomical fingerprints, which reveal subgroups that show differences in clinical measures. The study presents an analytical framework for linking neurodevelopmental and clinical diversity in autism to underlying molecular mechanisms, thus highlighting the need for personalized support strategies.

https://doi.org/10.1016/j.bpsc.2025.07.001

There is increasing recognition that most neurodevelopmental conditions are highly heterogeneous at both the mechanistic and phenotypic levels (1). Therefore, understanding heterogeneity is vital for uncovering underlying mechanisms that could pave the way for targeted, personalized support (2,3). This applies to autism, a neurodevelopmental condition characterized by 1) differences in social communication and interaction, 2) the presence of repetitive and stereotyped behaviors, and 3) altered sensory processing (4). These traits typically emerge during early childhood and are accompanied by differences in brain anatomy (5). While the neuroanatomy of autism is highly diverse, imaging transcriptomics studies, linking brain imaging data to gene expression patterns, suggest that imaging-derived phenotypes (IDPs) in autism may be linked to molecular pathways implicated in autism etiology (6,7). This approach enables subgrouping of autistic individuals on both the neuroanatomical and transcriptomic levels to identify biologically informed subgroups that may be linked to underlying mechanisms and therefore inform future approaches for targeted support.

Previous studies have explored the link between in vivo neuroanatomy and cortical gene expression signatures in autism. Romero-Garcia *et al.* (8) reported that cortical thickness (CT) differences in autistic children are linked to genes involved in synaptic transmission pathways (9,10). These findings were replicated and extended in an independent cohort of children, adolescents, and adults (11). The authors demonstrated that cortical patterns reflecting differences in

CT are transcriptomically enriched for genes known to be involved in autism etiology that map onto synaptic transmission and cell adhesion pathways (11). Different gene enrichment patterns were observed across clinical autistic subgroups defined by their sensory profiles (12). This suggests that specific autism phenotypes may have a distinctive neuroanatomical signature or "fingerprint," which may relate to different molecular mechanisms.

To date, however, gene expression decoding, i.e., the analysis of spatial correlations between imaging and gene expression signatures, has mostly been restricted to IDPs representing group-level effects. Due to the high variability within the autistic population, group-level analyses may overlook individual differences (13). Therefore, more recent approaches have been developed to shift the analysis of statistical effects from the group level to the individual level. This includes normative modeling approaches, in which each individual is positioned relative to the neurotypical range of phenotypic diversity in brain structure (14,15). These studies show that autistic individuals may be subgrouped based on patterns of neuroanatomical deviations, with each subgroup showing different clinical profiles (16,17). Therefore, the examination of these neuroanatomical fingerprints rather than group differences may hold the key to subgrouping autism.

In this study, we used an imaging transcriptomics approach to subgroup autistic individuals based on the transcriptomic signature associated with their IDPs, characterized by CT. This analytical framework facilitates linking neuroanatomical and clinical diversity in autism to underlying mechanisms. We aimed to identify subgroups that differed in their neurobiology and symptomatology and might be linked to putative underlying mechanisms. Therefore, we examined a large and clinically diverse cohort of autistic individuals and control individuals recruited within the EU-AIMS (European Autism Interventions) LEAP (Longitudinal European Autism Project) (www.aims-2-trials.eu) (18). This study offers comprehensive phenotypic assessments of more than 700 individuals, including both males and females ages 6 to 30 years, with varying degrees of autistic traits (19). Therefore, the LEAP cohort is particularly well suited for subgrouping purposes. To link IDPs to gene expression signatures, a spatially dense (i.e., vertex-level) representation of the Allen Human Brain Atlas (AHBA) was generated characterizing each gene expression signature across the cortical surface. This allowed us to assess the spatial correlation between each brain phenotype and the cortical expression signatures. Subsequently, we stratified autistic individuals based on similarities in their IDP-associated transcriptomic profiles and compared the resulting subgroups on clinical characteristics. Last, we tested for an enrichment of the gene sets most strongly associated with the subgroups. This allowed us to 1) link neuroanatomical variability in autism to specific transcriptomic correlates and 2) determine the extent to which these correlates converged within and across subgroups.

METHODS AND MATERIALS

Participants

This study used data provided by the multicentered EU-AIMS LEAP. A comprehensive description of the sample has been published elsewhere (18,19). In brief, a total of 359 (101 female, 258 male) autistic individuals ages 6 to 30 years with structural magnetic resonance imaging (MRI) data were included (Table 1). A detailed description of inclusion/exclusion criteria, clinical assessments, and medication status has been provided elsewhere [see the Supplement and (11)]. Independent ethics committees approved the study, and written informed consent was obtained for all participants.

MRI Data Acquisition

All participants underwent MRI on 3T scanners located at 6 sites: University of Cambridge, United Kingdom; King's College London, United Kingdom; Central Institute of Mental Health, Mannheim, Germany; Radboud University Medical Centre, the Netherlands; University Medical Centre, Utrecht, the Netherlands; and Rome University, Italy. High-resolution structural T1-weighted volumetric images were acquired with full head coverage at 1.2-mm thickness with 1.2 × 1.2 mm^2 in-plane resolution (see the Supplement).

Cortical Surface Reconstruction Using FreeSurfer

FreeSurfer version 6.0.0 was used to obtain cortical surface representations for each T1-weighted image of 708 autistic and non-autistic individuals in the LEAP sample. These fully automated processes have been described in detail elsewhere (20,21). All surface reconstructions underwent quality assessments as outlined in Ecker *et al.* (11). In brief, surface reconstructions were rated by 3 independent raters, leading to the inclusion of 638 individuals (359 autistic, 279 nonautistic) (Table S2). We examined measures of CT, defined as the

Table 1. Participant Demographic Characteristics

					Statistics	
	Total Sample, N = 359	Subgroup 1A, n = 75	Subgroup 1B, n = 26	Subgroup 2, n = 258	F or χ^2	p
Age, Years	17.49 (5.52)	17.69 (5.85)	17.42 (5.71)	17.44 (5.42)	$F_2 = 0.06$	.94
IQ	98.92 (19.76)	97.71 (19.66)	102.92 (22.7)	98.87 (19.51)	$F_2 = 0.67$	.51
Mean CT, mm	2.28 (0.13)	2.66 (0.12)	2.72 (0.16)	2.68 (0.13)	$F_2 = 1.88$	.16
Sex						
Female	101 (28.1%)	25 (33.3%)	2 (7.7%)	74 (28.7%)	$\chi^2_2 = 6.41$	.04
Male	258 (71.9%)	50 (66.7%)	24 (92.3%)	184 (71.3%)		
Site	–	–	–	–	$\chi^2_{10} = 8.25$	.6

Values are presented as mean (SD) or n (%).
CT, cortical thickness.

shortest distance from the outer to the inner boundary at each vertex (22), smoothed using a 15-mm kernel to enhance the signal-to-noise ratio and be consistent with previous research (11,23,24). For each participant, we also computed the average CT across the cortex (CT_0).

To make individuals comparable, IDPs were standardized within the neurotypical range of control participants by means of a general linear model (GLM) that included both linear and quadratic age, sex, full scale IQ (FSIQ), acquisition site, and CT_0 as predictors (X). The model coefficients (β_{TD}) were subsequently used to predict CT across the cortex for all individuals in our cohort ($\hat{Y} = X\beta_{TD}$). The resulting residuals (res = $Y - \hat{Y}$) were centered and scaled based on the neurotypical CT distribution, thus expressing all data in unit standard deviations of the predicted neurotypical mean (z_{res}). Thus, instead of using absolute CT metrics, all datasets were normalized to unit standard deviations relative to the canonical trajectory (Figure 1, step 1).

Transcriptomic Decoding of IDPs

To link IDPs to gene expression patterns, we initially generated a spatially dense (i.e., vertex-level) representation of the AHBA human brain transcriptome as described by Gryglewski *et al.* (25). The AHBA data was quality assessed using the *abagen* toolbox (26) and mapped onto the FreeSurfer *fsaverage6* template. Messenger RNA expression values for vertices without AHBA representation were predicted via spatial interpolation using Gaussian process regression (i.e., ordinary Kriging). To account for the complex pattern of cortical folding, spatial interpolation was performed based on existing AHBA samples located within a geodesic neighborhood of 40 mm (see Transcriptomic Alignment Between Imaging Phenotypes and Gene Expression Patterns in Supplemental Methods for details). This resulted in spatially smooth gene expression maps for >15,600 genes measured in cortical brain tissue. Subsequently, we assessed the spatial correlations between each of the 359 standardized IDPs and the expression profiles of 15,633 genes (Figure 1, step 2).

The statistical assessment of spatial correlations was conducted within the framework of spatial-autocorrelation (α) preserving null modeling (27), using the variogram matching approach developed by Burt *et al.* (28). Given the high computational demands of this approach, we used principal component analysis to decompose the matrix of normalized gene expression maps into a set of 9 coexpression gradients with eigenvalues >1, which captured 41% of the total variability in gene expression across the cortex. For each gradient, a total of 1000 α-preserving null models were then precomputed to characterize the empirical distribution of spatial correlations under the null hypothesis, following *knn*-parameter optimization (28). This allowed us to derive a nonparametric α-corrected p value estimate for each gene based on the null distribution of spatial correlations with its respective gradient pattern. Gene-level p values were subsequently adjusted for multiple comparisons using the empirical cumulative density function of the extreme value distribution of spatial correlations across gradient nulls (29) (see Transcriptomic Decoding of Surface-Based IDPs in Supplemental Methods for details) (Figure 1, step 3).

Clustering of IDPs Based on Transcriptomic Profiles

The matrix of absolute spatial correlations between IDPs and cortical gene expression patterns (359 IDPs × 15,633 genes) served as input to a k-means clustering algorithm to identify subgroups of participants (and genes) with a similar IDP-related transcriptomic profile. Here, the optimal number of clusters was identified using the R package *NbClust* (version 3.0.1) using the complete aggregation method, which evaluates clustering solutions for different numbers of clusters across multiple validity indices [see the Supplement and (30)]. The stability of the clusters was assessed using the *clusterboot* function implemented in the R package *fpc* (version 2.2.9) (31), which performs bootstrap resampling of the data and evaluates the stability of each cluster by calculating Jaccard coefficients that represent the similarity between original clustering and bootstrapped clustering, with a Jaccard similarity value of >0.75 generally indicating a stable clustering solution (32) (Figure 1, step 4).

Subgroup Differences in Clinical Measures

For further characterization of the subgroups with regard to the clinical measures, we used analyses of covariance and post hoc t tests to compare clinical measures between subgroups. We covaried for age, IQ, site, and biological sex to assess subgroup differences independent of demographic factors. All subgroup differences between clinical measures were corrected for multiple comparisons using Bonferroni correction (33). Autistic traits were assessed using the Autism Diagnostic Observation Schedule (34), Autism Diagnostic Interview-Revised (ADI-R) (35), Repetitive Behavior Scale-Revised (RBS-R) (36), Social Responsiveness Scale, Second Edition (37), and the Short Sensory Profile (SSP) (38). Co-occurring attention-deficit/hyperactivity disorder (ADHD) was assessed using the parent- and self-reported DSM-5–based ADHD Rating Scale (4). The Beck Anxiety Inventory (39) adult and youth self-report versions were used to assess levels of anxiety. The Beck Depression Inventory-II adult and youth self-report versions were used (40,41) to assess the severity of depressive symptoms (Figure 1, step 5). For all clinical scales, missing data were imputed wherever possible to achieve a maximum sample size [see (42) for details].

Surface-Based Statistical Analyses of CT

The vertex-level statistical analyses were conducted using the SurfStat toolbox for MATLAB (version R2021a; The MathWorks, Inc.) and R (43). Vertexwise between-subgroup differences in CT (Y) were examined with a GLM incorporating

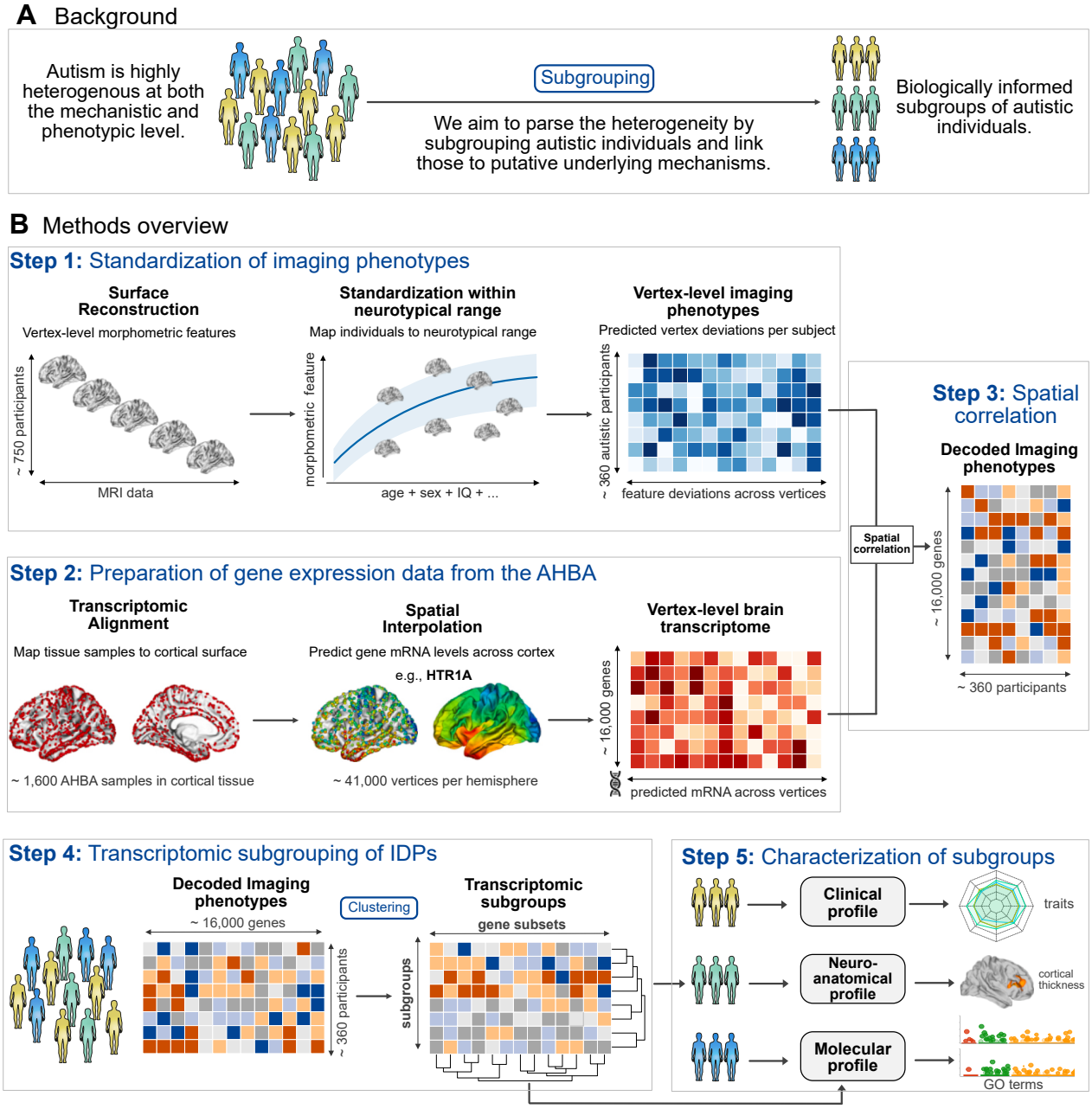

Figure 1. Schematic overview of the analytical framework. **(A)** Schematic overview of the background of the study. **(B)** Schematic overview of the methods of the study consisting of transcriptomic alignment between standardized IDPs (step 1) and gene expression data provided by the AHBA (step 2) via spatial correlation (step 3) and clustering of IDPs based on similarities in transcriptomic associations (step 4), with subsequent clinical and molecular characterization (step 5). AHBA, Allen Human Brain Atlas; GO, gene ontology; IDP, imaging-derived phenotype; MRI, magnetic resonance imaging; mRNA, messenger RNA.

subgroup, sex, and acquisition site as fixed effect factors and age, quadratic age, FSIQ, and CT_0 as continuous covariates, while ε_i is the residual error at vertex *i*.

$$Y_i = \beta_0 + \beta_1 \text{Subgroup} + \beta_2 \text{Sex} + \beta_3 \text{Age} + \beta_4 \text{Age}^2 + \beta_5 \text{FSIQ} + \beta_6 \text{Site} + \beta_7 \text{CT} + \varepsilon_i \quad (1)$$

Between-subgroup differences were estimated from the coefficient β_1, normalized by the standard error. All continuous covariates were mean centered. Corrections for multiple comparisons were performed using random field theory–based cluster analysis for nonisotropic images with a cluster-based significance threshold of .05 (2 tailed) (44).

Molecular Characterization of Subgroups Using Gene-Set Enrichment Analysis

To link subgroups to mechanisms, gene-set enrichment analyses were performed to annotate each subgroup based on the gene sets most representative of each subgroup. Therefore, we used the gene sets with the highest average correlations obtained through clustering. These subsets contained the most significant genes based on the absolute correlations, thresholded at $p_{adjusted} < .01$. Initially, we tested these gene sets for enrichment of genes known to be involved in the etiology of autism including genes with rare and de novo variants (45), differentially expressed genes (DEGs) (46), and coexpression modules that mediate typical brain development in autism (47). Additionally, we tested for an enrichment of gene ontology (GO) terms. For details about the gene-set enrichment analyses, see Molecular Characterization of Subgroups Using Gene Enrichment Analysis in Supplemental Methods.

RESULTS

Subgrouping of IDPs Based on Similarities in Transcriptomic Signatures

Gene expression decoding of standardized IDPs resulted in a participant × gene (359 × 15,633) matrix of spatial correlations (Figure 2A) representing the absolute strength of the transcriptomic associations between IDPs and cortically expressed genes and was subsequently utilized for data-driven, unsupervised k-means clustering. We discerned an optimal bifurcated clustering solution with a mean bootstrapped Jaccard similarity index of 0.95 and 0.98, subdividing participants into two subgroups: one group of individuals (subgroup 1) with an average moderate degree of transcriptomic associations (n = 101; 27 female and 72 male; mean absolute $r_{spatial}$ = 0.13) and one group (subgroup 2) with a low average degree of transcriptomic correlations (n = 258; 74 female and 184 male; $\bar{r}_{spatial}$ = 0.07) (Figure 2A). Clustering across genes revealed 4 gene sets (gene sets 1–4), with Jaccard indices of 0.96, 0.95, 0.93, and 0.95, respectively.

To further investigate the putative underlying mechanisms in individuals with a moderate degree of transcriptomic correlations, a second-level clustering was performed across subgroup 1, delineating 2 subgroups, subgroup 1A (n = 75; 25 female and 50 male) and subgroup 1B (n = 26, 2 female and 24 male), with a mean bootstrapped Jaccard similarity index of 0.96 and 0.99, respectively. Each of the 3 subgroups was linked to gene sets, i.e., subgroup 1A showed low to moderate transcriptomic associations with gene set 1 ($\bar{r}_{spatial}$ = 0.16) (Figure 2A). Individuals in subgroup 1B exhibited the highest spatial correlations with genes in gene set 1 ($\bar{r}_{spatial}$ = 0.26) and gene set 4 ($\bar{r}_{spatial}$ = 0.18) (Figure 2A). In contrast, individuals in subgroup 2 exhibited low correlations across all 4 gene sets (Figure 2A). There were no subgroup differences in age (F_2 = 0.06, p = .94), FSIQ (F_2 = 0.67, p = .51), or mean CT (F_2 = 1.88, p = .16). However, the male-to-female ratio was significantly lower in subgroup 1B (χ^2_2 = 6.41, p = .04) (Table 1). Therefore, we covaried for these measures (age, FSIQ, sex, site, and mean CT) in all subsequent analyses. Overall, we found 3 participant subgroups that were differentially associated with the 4 gene sets.

Subgroup Differences in Clinical Phenotypes

Next, we examined differences in clinical measures between subgroups. There was a significant main effect of subgroup on the communication domain of the ADI-R (F = 3.9, p = .03) and on the RBS-R (F = 3.14, p = .04) (Figure 3A). Individuals in subgroup 1B had lower symptom scores compared with individuals in subgroup 1A or 2. There were significant subgroup differences in sensory symptoms, particularly on the taste subscale of the SSP (F = 4.22, p = .02) (Figure 3B). Thus, individuals in subgroup 1B, who exhibited the strongest transcriptomic associations, showed significantly lower symptom scores than individuals in other subgroups, confirmed by post hoc t tests (Figure 3F). However, there were no significant differences in co-occurring symptoms or other autistic traits (Table S4).

Neuroanatomical Differences Between Subgroups

Subgroups also differed significantly in CT. There was a significant main effect of subgroup in the left temporal pole (approximately Brodmann area [BA] 36/38) (Figure S4). Furthermore, individuals in subgroup 1A had significantly increased CT in the left isthmus cingulate cortex and the left posterior cingulate cortex (BA 23/24) compared with individuals in subgroups 1B and 2. Additionally, individuals in subgroup 1A showed significantly increased CT in the right middle frontal gyrus (BA 9/44/45) and decreased CT in the left posterior cingulate cortex (BA 23/31), the left temporal pole

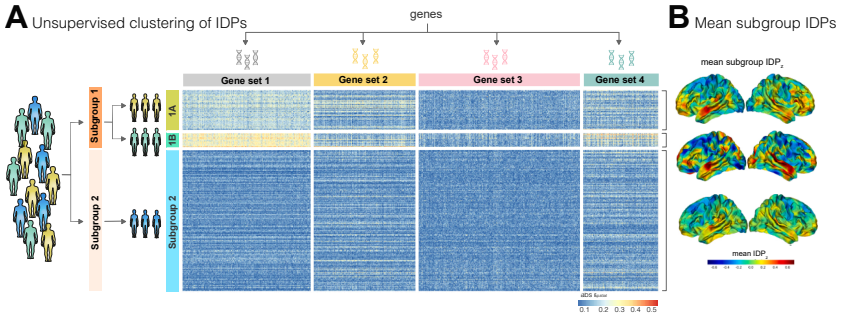

Figure 2. Subgrouping results. **(A)** Heatmap of absolute spatial correlations ($r_{spatial}$) between each standardized IDP and the cortical expression signatures of 15,633 protein-coding genes. Subfields result from a 2-step clustering solution (k-means) that initially subdivided participants into a group with medium to high transcriptomic associations (subgroup 1) and a group with low to medium transcriptomic associations (subgroup 2). Second-level clustering further subdivided individuals in subgroup 1 into subgroup 1A and subgroup 1B, with differential transcriptomic associations with gene set 1 and gene set 4, respectively. **(B)** Average standardized IDPs within subgroups (IDP$_z$). z indicates normalized deviations from the typical developmental trajectory of cortical thickness. IDP, imaging-derived phenotype.

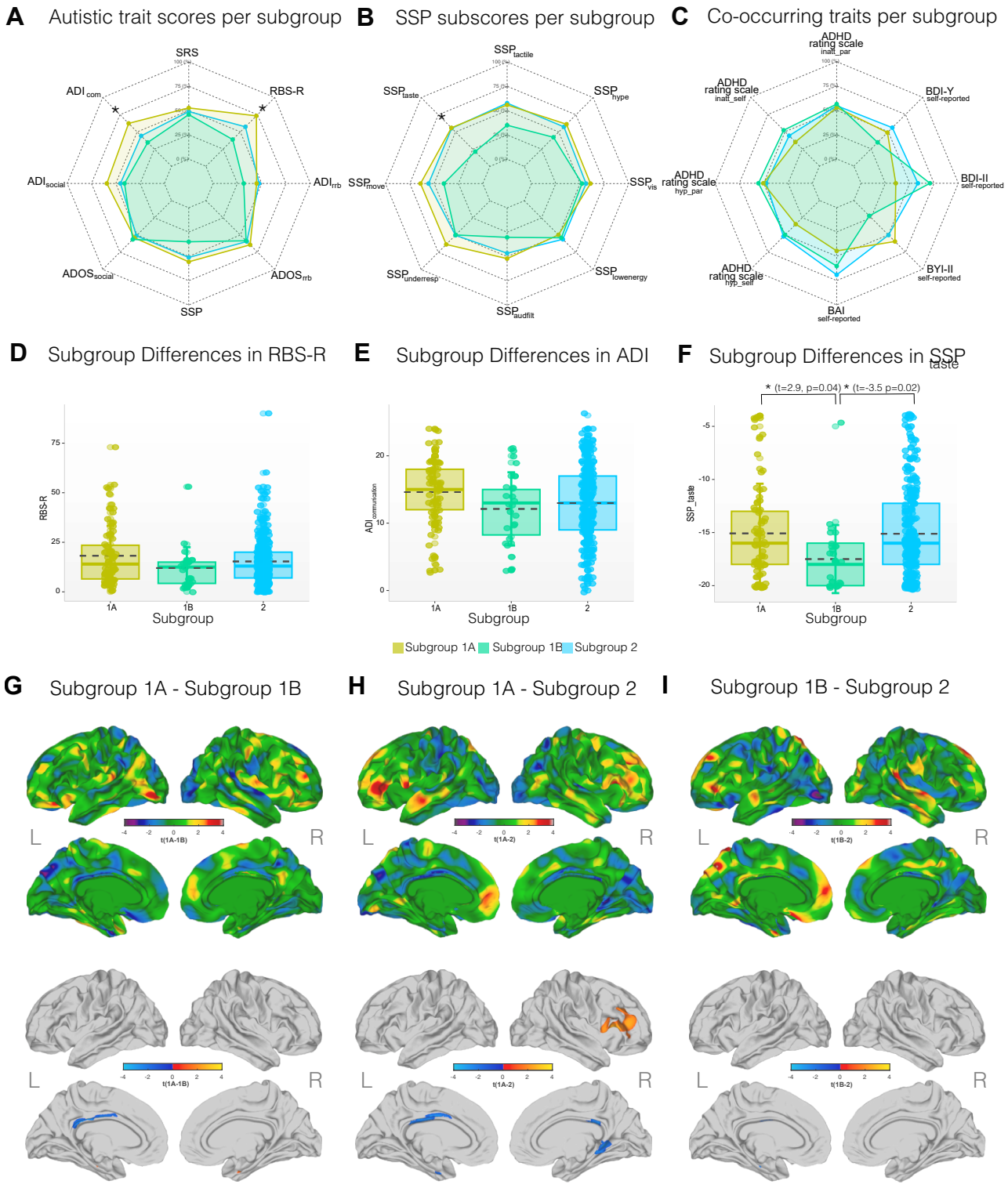

Figure 3. Clinical characterization of transcriptomic subgroups. **(A)** Subgroup differences in autism symptoms as measured by the SRS-2, RBS-R, ADI-R, ADOS, and SSP. Note. For all clinical scales, significant differences are marked by an asterisk (*), based on $p < .05$. **(B)** Subgroup scores on the SSP. **(C)** Differences in co-occurring traits measured using the ADHD Rating Scale, BAI, BYI-II, BDI-II, and BDI-Y. **(D)** Subgroup differences in the RBS-R, using a post hoc *t* test. **(E)** Subgroup differences in the communication domain of the ADI-R, using a post hoc *t* test. **(F)** Significant subgroup differences on the taste item

(BA 36/38), and the right isthmus cingulate cortex (BA 24) compared with individuals in subgroup 2 (Figure 3F–H and Table S3).

Molecular Characterization of Subgroups

We tested the gene sets with the highest absolute transcriptomic associations with the subgroups using gene-set enrichment analysis. The 3 resulting subsets consisted of significant genes only ($p_{adjusted} < .01$). Gene subset A contained 1221 genes significantly associated with subgroup 1A. Gene subsets B and C were associated with subgroup 1B and consisted of 1340 and 65 genes, respectively (Figure 4A). Of these subsets, only subsets A and B were significantly enriched for autism candidate genes and DEGs in autism (Figure 4B). Gene subset A was significantly enriched for up- and downregulated genes in autism that have previously been associated with GO terms that represent synaptic functioning and neuronal signals (9,46). Gene subset B was enriched for DEGs linked to synaptic functioning and transmembrane activity and for SFARI (Simons Foundation Autism Research Initiative) autism genes (46) (Figure 4B).

Next, we tested the enrichment of genes in coexpression modules that mediate typical brain development (47). Notably, all gene subsets showed a significant enrichment for coexpression module M2, associated with synaptic transmission, which exhibits peak expression during early childhood and adolescence (Figure 4C). The same applies to synaptic transmission module M15, which was significantly enriched in gene subsets A and B. We observed a significant enrichment of module M20, which is linked to zing-finger proteins and transcription factors (TFs) (47). Unlike synaptic modules, coexpression modules representing TFs exhibit peak expression during prenatal brain development and show the lowest expression levels during childhood (Figure 4D). Lastly, in gene subset B linked to subgroup 1B, we observed an enrichment of modules M8 (neuronal development TFs) and M16 (cell adhesion signaling), with peak expression during the prenatal stage and during childhood/adolescence. Overall, IDPs in autism converge onto the coexpression signatures of specific transcriptional programs that impact brain development at different developmental stages.

Lastly, we annotated subgroup 1A and subgroup 1B by testing for an enrichment of general GO terms. Therefore, we extracted the genes from gene subset A that were exclusively associated with subgroup 1A (gene subset $1A_{only}$) and subset B genes that were only associated with subgroup 1B (gene subset $1B_{only}$). This resulted in 657 genes for gene subset $1A_{only}$ and 776 genes for gene subset $1B_{only}$. The subgroups differed in terms of enrichment profiles, with subset $1A_{only}$ showing a stronger enrichment of biological processes and gene subset $1B_{only}$ showing a stronger enrichment of cellular component terms (Figure 4E, F and Table S7).

DISCUSSION

In this study, we used an imaging transcriptomics approach to dissect autism heterogeneity based on the transcriptomic signatures associated with individual IDPs. Additionally, the derived subgroups were characterized in terms of clinical, neuroanatomical, and molecular measures. We established that 1) subgroups differed on the clinical, neuroanatomical, and molecular levels and that 2) subgroups converged onto different putative molecular mechanisms. These findings highlight mechanistic and phenotypic differences between subgroups of autistic individuals, providing a framework to further elucidate the variability within autism.

Within this framework, we initially transcriptomically decoded the structural IDPs from 359 autistic individuals, using spatially dense representations of the AHBA transcriptome. The individual's neurophenotypes were characterized based on measures of CT, a morphometric feature known to be influenced by both genetic variation and differences in gene expression (48,49). Differences in CT in autism are well documented and have been linked to its molecular etiology (8,11). Our study indicates that the transcriptomic profiles associated with IDPs in autism vary across individuals. This finding is consistent with previous reports suggesting that each person's neuroanatomy is marked by individualized patterns of neuroanatomical deviations from the typical trajectory of brain development, i.e., a neuroanatomical fingerprint (16). Thus, rather than analyzing absolute measures of CT, we standardized IDPs within the neurotypical range prior to decoding using an age- and sex-matched sample of control participants recruited at the same acquisition sites. This standardization of IDPs is an important step, as it makes it possible to perform comparative analyses across demographically diverse phenotypes and focus on interindividual differences rather than on group mean differences. This approach allows accounting for interindividual variability due to demographic and technical confounds. It thus places all data within the broader context of neurodiversity (50) and is consistent with previous approaches (14,15,51) emphasizing the conceptual relevance of elucidating neurodiversity in autism. This approach is particularly well suited for subgrouping purposes.

Using unsupervised clustering approaches, we subdivided individuals based on similarities in their IDP-related transcriptomic profiles. We discerned 3 subgroups that were differentially associated with 4 different gene sets. The strongest transcriptomic associations were observed in individuals within subgroup 1B. Most individuals exhibited small spatial associations between IDPs and gene expression

of the SSP, using a post hoc *t* test. **(G)** Subgroup differences in CT between subgroup 1A and subgroup 1B. **(H)** Subgroup differences in CT between subgroup 1A and subgroup 2. **(I)** Subgroup differences in CT between subgroup 1B and subgroup 2. For all surface-based statistical patterns, the upper panels show the *t* test statistic (unthresholded) associated with each subgroup contrast. The lower panels indicate clusters with significantly increased (orange) and decreased (blue) CT for the respective subgroup comparison (random field theory–based cluster-corrected $p < .05$, 2 tailed). ADI-R, Autism Diagnostic Interview-Revised; ADOS, Autism Diagnostic Observation Schedule; BAI, Beck Anxiety Inventory; BDI-II, Beck Depression Inventory-II; BDI-Y, Beck Depression Inventory for Youth; BYI-II, Beck Anxiety Inventory for Youth-II; CT, cortical thickness; L, left hemisphere; R, right hemisphere; RBS-R, Repetitive Behavior Scale-Revised; SRS, Social Responsiveness Scale; SSP, Short Sensory Profile.

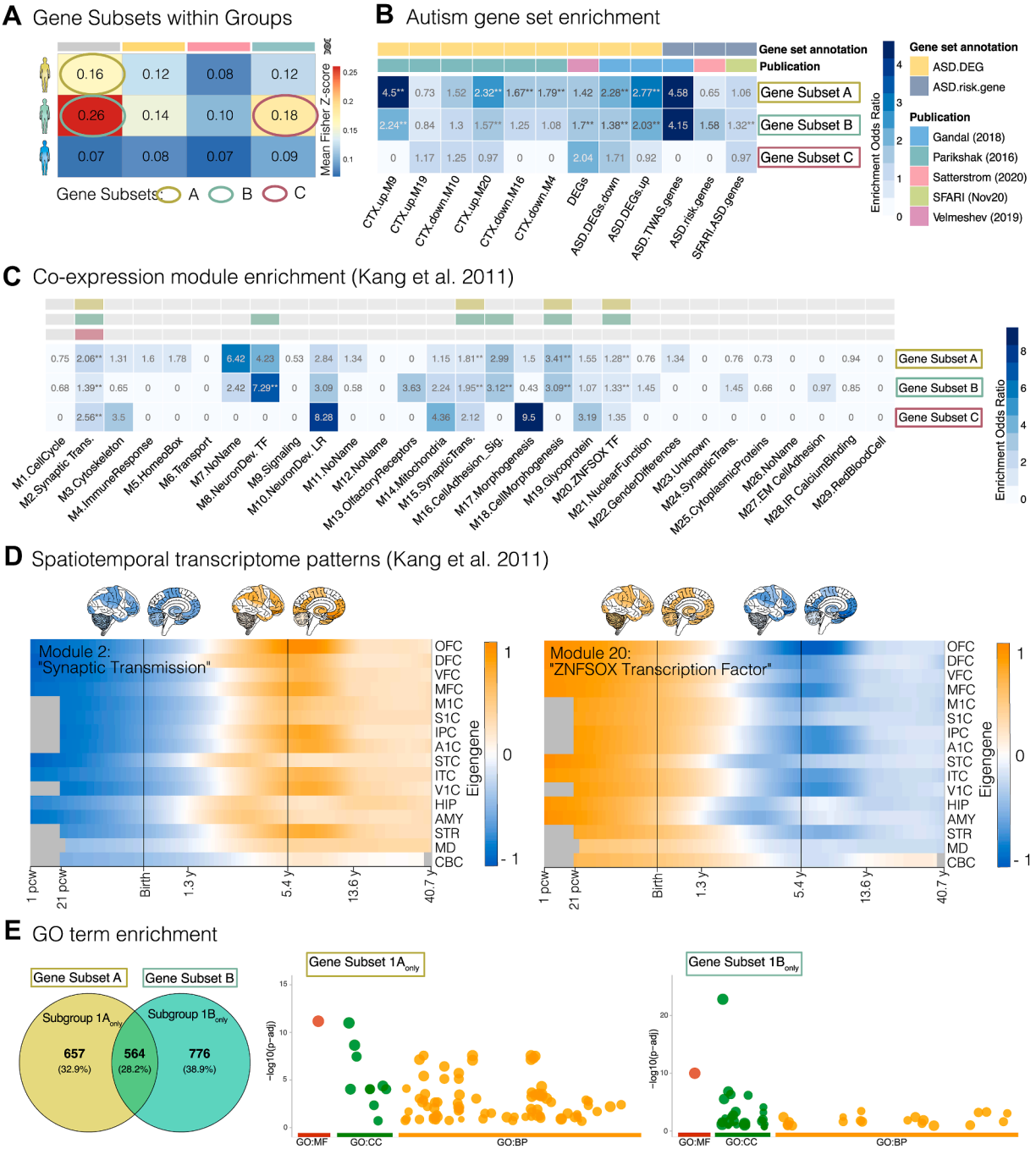

Figure 4. Gene-set enrichment analysis. **(A)** Average absolute spatial correlations (Fisher's *z* transformed) within subgroups, resulting in 3 gene subsets labeled A (yellow), B (green), and C (red). **(B)** Odds ratios at a false discovery rate–corrected $p_{adjusted}$ threshold of .01 resulting from the gene-set enrichment analyses for genes expressed in gene subsets A, B, and C, respectively. Gene sets were subdivided into sets with differential gene expression in autism and sets representing autism likelihood genes. Gene sets are annotated and labeled based on their original publication. **(C)** Enrichment of genes mediating typical brain development as reported in the spatiotemporal transcriptome dataset provided by Kang *et al.* (47). Set names contain their respective coexpression module label (e.g., M1) followed by their functional description based on their GO term enrichment. **(D)** Spatiotemporal expression profiles of brain gene modules that were significantly enriched in the gene subsets for module 2 (synaptic transmission) and module 20 (ZNFSOX transcription factor). The x-axis shows the developmental time frame (pcw), and the y-axis shows the different brain regions. **(E)** Venn diagram showing the number of shared and distinct genes from subsets A and B, resulting in gene subset $1A_{only}$ (significantly associated with subgroup 1A exclusively) and gene subset $1B_{only}$ (significantly associated with subgroup 1B exclusively) (left). The middle and right panels indicate the functional enrichment of GO terms for gene subset $1A_{only}$ and gene subset $1B_{only}$, respectively. Up and down indicate upregulated and downregulated expression in autism, respectively. Summary statistics and details for all enriched terms are listed in Tables S6 and S7. A1C, primary auditory cortex; AMY, amygdala; ASD, autism spectrum disorder; BP, biological process; CBC,

signatures, as was characteristic of subgroup 2. Therefore, autistic individuals differ in both the magnitude and nature of the transcriptomic associations, further substantiating the growing evidence of significant heterogeneity in autism on the phenotypic and mechanistic level (13,52). These differences cannot be accounted for by variations in participant demographic characteristics such as age and IQ. However, there was a significant difference in the male-to-female ratio, with a higher proportion of males in subgroup 1B. Therefore, we controlled for biological sex to reduce potential demographic confounding and observed that participants in subgroup 1B exhibited lower levels of symptom severity in social communication, repetitive behaviors, and sensory symptoms but not in co-occurring symptoms (e.g., anxiety, depression, ADHD). Previous research suggests that sex differences are a factor that contributes to the heterogeneity in autism (53). Thus, our findings need to be interpreted in this context (54), and future research on the interaction between sex, transcriptomic profiles, and clinical measures is needed. Our findings suggest that autistic individuals with a higher association with gene expression patterns exhibit less severe symptoms overall. This may be because typical brain development is governed by various transcriptional programs—temporally and spatially coordinated patterns of gene expression guiding the formation of the nervous system, i.e., processes such as neurogenesis, axon guidance, and synapse formation (47). Therefore, changes in these programs are likely to impact the formation of the brain's neurocircuitry and have been implicated in the etiology of autism through genetic and transcriptomic investigations (46,55).

Coexpression networks were also implicated by our study. We found that the IDPs of individuals in subgroup 1 (i.e., the subgroup with the highest transcriptomic associations) were significantly associated with the gene expression signatures of genes previously reported to be up- and downregulated in the autism cortex (9,46). These included module CTX.M20, which contains genes implicated in the development and regulation of cell differentiation (9). Moreover, we found an enrichment of the gene coexpression modules that mediate typical brain development (47). This includes modules M2 and M15, which map onto synaptic transmission pathways, as well as modules M8 and M20, which are enriched for GO categories related to TFs (9). Notably, M2 and M20 follow opposite developmental trajectories across brain regions, with M20 being most active during prenatal brain development and M2 being most expressed during childhood. Taken together, our results suggest that different coexpression networks influence brain maturation across developmental states in a region-specific manner and that autistic individuals with neuroanatomical characteristics, spatially more closely aligned with these large-scale transcriptomic gradients, may exhibit greater resilience.

Our study's strengths include the combination of imaging and transcriptomics data; the large, heterogeneous, and deep-phenotyped dataset; and our analytical framework for parsing autism heterogeneity. However, there are limitations to this study. So far, we have not examined genomic variation that could underpin differential gene expression. Thus, it remains to be established how genetic variation influences gene expression in autism. We utilized the AHBA (56) data, which is the most comprehensive gene expression atlas to date. Nevertheless, the AHBA is based on adult donors, while we examined IDPs of children, adolescents, and adults. Therefore, we acknowledge the importance of repeating our analyses in age-matched samples to corroborate the relationship between genetic variation, gene expression, and neurodiversity in autism.

Conclusions

We identified subgroups within a sample of autistic participants based on the link between brain phenotypes and gene expression profiles. These subgroups showed differences in clinical measures and neuroanatomy. They also varied in their underlying genetic profiles, highlighting the biological heterogeneity in autism and therefore the need to develop more targeted support strategies.

ACKNOWLEDGMENTS AND DISCLOSURES

This work was supported by the Innovative Medicines Initiative 2 Joint Undertaking (IHI-JU2) (Grant Agreement No. 115300) for the EU-AIMS and the AIMS-2-TRIALS projects (Grant No. 777394 [to DM]). This Joint Undertaking receives support from the European Union's Horizon 2020 research and innovation program and the European Federation of Pharmaceutical Industries and Associations and AUTISM SPEAKS, Autistica, SFARI. CE gratefully acknowledges support from the German Research Foundation (DFG) (Project No. 551579379), the Rolf M. Schwiete Stiftung (Project No. 2024-022), and the DYNAMIC center funded by the LOEWE program of the Hessian Ministry of Science and Arts (Grant No. LOEWE1/16/519/03/09.001(0009)/98). Moreover, this work was supported by the DFG-funded Transregio Aggression (TRR 379) (Project No. 512007073). DM also acknowledges support from the National Institute for Health Research Maudsley Biomedical Research Centre. Furthermore, this work has received funding from Horizon Europe (Grant Agreement No. 101057385) and UK Research and Innovation under the UK government's Horizon Europe funding guarantee (Grant No. 10039383) (R2D2-MH). The IHI-JU2 had no role in the design of the study; the collection, analysis, or interpretation of data; the writing of the article; or the decision to publish the results. Any views expressed are those of the author(s) and not necessarily those of the IHI-JU2.

We gratefully acknowledge the contributions of the EU-AIMS LEAP Group: Jumana Ahmad, Sara Ambrosino, Bonnie Auyeung, Tobias Banaschewski, Simon Baron-Cohen, Sarah Baumeister, Christian F. Beckmann, Sven Bölte, Thomas Bourgeron, Carsten Bours, Michael Brammer, Daniel Brandeis, Claudia Brogna, Yvette de Bruijn, Jan K. Buitelaar, Bhismadev Chakrabarti, Tony Charman, Ineke Cornelissen, Daisy Crawley, Flavio Dell'Acqua, Guillaume Dumas, Sarah Durston, Christine Ecker, Jessica Faulkner, Vincent Frouin, Pilar Garcés, David Goyard, Lindsay Ham, Hannah Hayward, Joerg Hipp, Rosemary Holt, Mark H. Johnson, Emily J.H. Jones, Prantik Kundu, Meng-Chuan Lai, Xavier Liogier D'ardhuy, Michael V. Lombardo, Eva Loth, David J. Lythgoe, René Mandl, Andre Marquand, Luke Mason, Maarten Mennes, Andreas Meyer-Lindenberg, Carolin Moessnang, Nico Bast, Declan G.M. Murphy, Bethany Oakley, Laurence O'Dwyer, Marianne Oldehinkel, Bob Oranje, Gahan Pandina, Antonio M. Persico,

cerebellar cortex; CC, cell compartment; CTX, cortex; DEG, differentially expressed gene; DFC, dorsolateral prefrontal cortex; GO, gene ontology; HIP, hippocampus; IPC, posterior inferior parietal cortex; ITC, inferior temporal cortex; M1C, primary motor cortex; MD, mediodorsal nucleus of the thalamus; MF, molecular function; MFC, medial prefrontal cortex; OFC, orbital prefrontal cortex; pcw, postconception week; S1C, primary somatosensory cortex; STC, superior temporal cortex; STR, striatum; V1C, primary visual cortex; VFC, ventrolateral prefrontal cortex.

Barbara Ruggeri, Amber Ruigrok, Jessica Sabet, Roberto Sacco, Antonia San José Cáceres, Emily Simonoff, Will Spooren, Julian Tillmann, Roberto Toro, Heike Tost, Jack Waldman, Steve C.R. Williams, Caroline Wooldridge, and Marcel P. Zwiers. The primary contact for the EU-AIMS LEAP Group is Declan G. Murphy (pa-dmurphy@kcl.ac.uk).

During the past 3 years, JKB has been a consultant to, member of advisory board of, and/or speaker for Janssen-Cilag B.V., Takeda/Shire, Roche, Novartis, Medice, Angelini, and Servier. He is not an employee of any of these companies and is not a stock shareholder of any of these companies. TB has served in an advisory or consultancy role for eye level, Infectopharm, Medice, Neurim Pharmaceuticals, Oberberg GmbH, and Takeda. He has received conference support or speaker's fees from Janssen-Cilag, Medice, and Takeda. He has received royalties from Hogrefe, Kohlhammer, CIP Medien, and Oxford University Press. The current work is unrelated to the grants and relationships mentioned above. TC has received research grant support from the Medical Research Council (United Kingdom), the National Institute for Health Research, Horizon 2020 and the Innovative Medicines Initiative (European Commission), MQ, Autistica, FP7 (European Commission), the Charles Hawkins Fund, and the Waterloo Foundation. He has served as a consultant to F. Hoffmann-La Roche Ltd. and Servier. He has received royalties from Sage Publications and Guilford Publications. DM has received consultancy fees from Roche and Servier and grant support from the Medical Research Council (United Kingdom), the National Institute for Health Research, and Horizon 2020 and the Innovative Medicines Initiative (European Commission). EJHJ has received funding from Action Medical Research, EU Horizon 2020, the Innovative Medicines Initiative, the Medical Research Council (United Kingdom), MQ: Transforming Mental Health, and the Economic and Social Research Council. All other authors report no biomedical financial interests or potential conflicts of interest.

ARTICLE INFORMATION

From the Department of Child and Adolescent Psychiatry, University Hospital, Goethe University, Frankfurt am Main, Germany (JL, CG, LMB, HS, BH, TS, AGC, CE); Brain Imaging Center, Goethe University, Frankfurt am Main, Germany (JL, CG, LMB, HS, BH, TS, CE); Department of Biosciences, Goethe University Frankfurt, Frankfurt am Main, Germany (JL, LMB); Department of Forensic and Neurodevelopmental Sciences, Institute of Psychiatry, Psychology and Neuroscience, King's College London, London, United Kingdom (CMP, EL, BO, DM, CE); Department of Cognitive Neuroscience, Donders Institute for Brain, Cognition and Behaviour, Radboud University Nijmegen Medical Center, Nijmegen, the Netherlands (JKB, CFB); Department of Psychology, Institute of Psychiatry, Psychology and Neuroscience, King's College London, London, United Kingdom (TC); Institut Pasteur, Human Genetics and Cognitive Functions Unit, Paris, France (TB, EB); Child and Adolescent Psychiatry, Central Institute of Mental Health, University of Heidelberg, Medical Faculty Mannheim, Mannheim, Germany (TB); and Centre for Brain and Cognitive Development, Birkbeck, University of London, London, United Kingdom (EJHJ).

Address correspondence to Johanna Leyhausen, M.Sc., at Leyhausen@med.uni-frankfurt.de.

Received Jun 2, 2025; revised Jun 6, 2025; accepted Jul 3, 2025.

Supplementary material cited in this article is available online at https://doi.org/10.1016/j.bpsc.2025.07.001.

REFERENCES

1. Wardenaar KJ, de Jonge P (2013): Diagnostic heterogeneity in psychiatry: Towards an empirical solution. BMC Med 11:201.
2. Loth E, Spooren W, Murphy DG, EU-AIMS Consortium (2014): New treatment targets for autism spectrum disorders: EU-AIMS. Lancet Psychiatry 1:413–415.
3. Loth E, Spooren W, Ham LM, Isaac MB, Auriche-Benichou C, Banaschewski T, *et al.* (2016): Identification and validation of biomarkers for autism spectrum disorders. Nat Rev Drug Discov 15:70–73.
4. American Psychiatric Association (2013): Diagnostic and Statistical Manual of Mental Disorders, Fifth Edition Washington, DC: American Psychiatric Association.
5. Ecker C, Bookheimer SY, Murphy DGM (2015): Neuroimaging in autism spectrum disorder: Brain structure and function across the lifespan. Lancet Neurol 14:1121–1134.
6. Arnatkeviciute A, Fulcher BD, Bellgrove MA, Fornito A (2022): Imaging transcriptomics of brain disorders. Biol Psychiatry Glob Open Sci 2:319–331.
7. Fornito A, Arnatkevičiūtė A, Fulcher BD (2019): Bridging the gap between connectome and transcriptome. Trends Cogn Sci 23:34–50.
8. Romero-Garcia R, Warrier V, Bullmore ET, Baron-Cohen S, Bethlehem RAI (2019): Synaptic and transcriptionally downregulated genes are associated with cortical thickness differences in autism. Mol Psychiatry 24:1053–1064.
9. Parikshak NN, Swarup V, Belgard TG, Irimia M, Ramaswami G, Gandal MJ, *et al.* (2016): Genome-wide changes in lncRNA, splicing, and regional gene expression patterns in autism. Nature 540:423–427.
10. Parikshak NN, Luo R, Zhang A, Won H, Lowe JK, Chandran V, *et al.* (2013): Integrative functional genomic analyses implicate specific molecular pathways and circuits in autism. Cell 155:1008–1021.
11. Ecker C, Pretzsch CM, Bletsch A, Mann C, Schaefer T, Ambrosino S, *et al.* (2022): Interindividual differences in cortical thickness and their genomic underpinnings in autism spectrum disorder. Am J Psychiatry 179:242–254.
12. Tillmann J, Uljarevic M, Crawley D, Dumas G, Loth E, Murphy D, *et al.* (2020): Dissecting the phenotypic heterogeneity in sensory features in autism spectrum disorder: A factor mixture modelling approach. Mol Autism 11:67.
13. Lombardo MV, Lai MC, Baron-Cohen S (2019): Big data approaches to decomposing heterogeneity across the autism spectrum. Mol Psychiatry 24:1435–1450.
14. Marquand AF, Rezek I, Buitelaar J, Beckmann CF (2016): Understanding heterogeneity in clinical cohorts using normative models: Beyond case-control studies. Biol Psychiatry 80:552–561.
15. Marquand AF, Kia SM, Zabihi M, Wolfers T, Buitelaar JK, Beckmann CF (2019): Conceptualizing mental disorders as deviations from normative functioning. Mol Psychiatry 24:1415–1424.
16. Zabihi M, Floris DL, Kia SM, Wolfers T, Tillmann J, Arenas AL, *et al.* (2020): Fractionating autism based on neuroanatomical normative modeling. Transl Psychiatry 10:384.
17. Zabihi M, Oldehinkel M, Wolfers T, Frouin V, Goyard D, Loth E, *et al.* (2019): Dissecting the heterogeneous cortical anatomy of autism spectrum disorder using normative models. Biol Psychiatry Cogn Neurosci Neuroimaging 4:567–578.
18. Charman T, Loth E, Tillmann J, Crawley D, Wooldridge C, Goyard D, *et al.* (2017): The EU-AIMS Longitudinal European Autism Project (LEAP): Clinical characterisation. Mol Autism 8:27.
19. Loth E, Charman T, Mason L, Tillmann J, Jones EJH, Wooldridge C, *et al.* (2017): The EU-AIMS Longitudinal European Autism Project (LEAP): Design and methodologies to identify and validate stratification biomarkers for autism spectrum disorders. Mol Autism 8:24.
20. Dale AM, Fischl B, Sereno MI (1999): Cortical surface-based analysis. I. Segmentation and surface reconstruction. Neuroimage 9:179–194.
21. Fischl B, Sereno MI, Dale AM (1999): Cortical surface-based analysis. II: Inflation, flattening, and a surface-based coordinate system. Neuroimage 9:195–207.
22. Fischl B, Dale AM (2000): Measuring the thickness of the human cerebral cortex from magnetic resonance images. Proc Natl Acad Sci U S A 97:11050–11055.
23. Seelemeyer H, Gurr C, Leyhausen J, Berg LM, Pretzsch CM, Schäfer T, *et al.* (2025): Decomposing the brain in autism: Linking behavioral domains to neuroanatomical variation and genomic underpinnings. Biol Psychiatry Cogn Neurosci Neuroimaging 10:1067–1077.
24. Arai T, Kamagata K, Uchida W, Andica C, Takabayashi K, Saito Y, *et al.* (2023): Reduced neurite density index in the prefrontal cortex of

adults with autism assessed using neurite orientation dispersion and density imaging. Front Neurol 14:1110883.
25. Gryglewski G, Seiger R, James GM, Godbersen GM, Komorowski A, Unterholzner J, *et al.* (2018): Spatial analysis and high resolution mapping of the human whole-brain transcriptome for integrative analysis in neuroimaging. Neuroimage 176:259–267.
26. Markello RD, Arnatkevičiūtė A, Poline JB, Fulcher BD, Fornito A, Misic B (2021): Standardizing workflows in imaging transcriptomics with the abagen toolbox. eLife 10:e72129.
27. Markello RD, Misic B (2021): Comparing spatial null models for brain maps. Neuroimage 236:118052.
28. Burt JB, Helmer M, Shinn M, Anticevic A, Murray JD (2020): Generative modeling of brain maps with spatial autocorrelation. Neuroimage 220:117038.
29. Ecker C, Pretzsch CM, Leyhausen J, Berg LM, Gurr C, Seelemeyer H, *et al.* (2025): Transcriptomic decoding of surface-based imaging phenotypes and its application to pharmacotranscriptomics. Nat Commun 16:6727.
30. Charrad M, Ghazzali N, Boiteau V, Niknafs A (2014): NbClust: An R package for determining the relevant number of clusters in a data set. J Stat Soft 61:1–36.
31. Hennig C (2024): fpc: Flexible Procedures for Clustering. Available at: https://cran.r-project.org/web/packages/fpc/index.html. Accessed August 6, 2024.
32. Hennig C (2007): Cluster-wise assessment of cluster stability. Comput Stat Data Anal 52:258–271.
33. Abdi H (2007): The Bonferroni and Šidák Corrections for Multiple Comparisons. Available at: http://www.utdallas.edu/∼herve/Abdi-Bonferroni2007-pretty.pdf. Accessed January 15, 2025.
34. Lord C, Risi S, Lambrecht L, Cook EH, Leventhal BL, DiLavore PC, *et al.* (2000): The autism diagnostic observation schedule-Generic: A standard measure of social and communication deficits associated with the spectrum of autism. J Autism Dev Disord 30:205–223.
35. Lord C, Rutter M, Le Couteur A (1994): Autism Diagnostic Interview-Revised: A revised version of a diagnostic interview for caregivers of individuals with possible pervasive developmental disorders. J Autism Dev Disord 24:659–685.
36. Lam KSL, Aman MG (2007): The repetitive behavior scale-revised: Independent validation in individuals with autism spectrum disorders. J Autism Dev Disord 37:855–866.
37. Constantino JN (2013): Social responsiveness scale. In: Volkmar FR, editor. Encyclopedia of Autism Spectrum Disorders. New York: Springer New York, 2919–2929.
38. Tomchek SD, Huebner RA, Dunn W (2014): Patterns of sensory processing in children with an autism spectrum disorder. Res Autism Spectr Disord 8:1214–1224.
39. Steer RA, Beck AT (1997): Beck Anxiety Inventory. In: Zalaquett CP, Wood RJ, editors. Evaluating Stress: A Book of Resources. Lanham, MD: Scarecrow Education, 23–40.
40. Beck AT (1996): Manual for the Beck Depression Inventory—II. Available at: https://cir.nii.ac.jp/crid/1370564063990947215. Accessed March 25, 2024.
41. Beck JS (2005): Beck youth inventories for children and adolescents. Manual. Available at: https://cir.nii.ac.jp/crid/1130282269408755072. Accessed March 25, 2024.
42. Llera A, Brammer M, Oakley B, Tillmann J, Zabihi M, Amelink JS, *et al.* (2022): Evaluation of data imputation strategies in complex, deeply-phenotyped data sets: The case of the EU-AIMS Longitudinal European Autism Project. BMC Med Res Methodol 22:229.
43. R Core Team (2021): R: A Language and Environment for Statistical Computing. Vienne, Austria: R Foundation for Statistical Computing. Available at: https://www.R-project.org/. Accessed February 14, 2024.
44. Worsley KJ, Andermann M, Koulis T, MacDonald D, Evans AC (1999): Detecting changes in nonisotropic images. Hum Brain Mapp 8:98–101.
45. Satterstrom FK, Kosmicki JA, Wang J, Breen MS, De Rubeis S, An JY, *et al.* (2020): Large-scale exome sequencing study implicates both developmental and functional changes in the neurobiology of autism. Cell 180:568–584.e23.
46. Gandal MJ, Zhang P, Hadjimichael E, Walker RL, Chen C, Liu S, *et al.* (2018): Transcriptome-wide isoform-level dysregulation in ASD, schizophrenia, and bipolar disorder. Science 362:eaat8127.
47. Kang HJ, Kawasawa YI, Cheng F, Zhu Y, Xu X, Li M, *et al.* (2011): Spatio-temporal transcriptome of the human brain. Nature 478:483–489.
48. Hofer E, Roshchupkin GV, Adams HHH, Knol MJ, Lin H, Li S, *et al.* (2020): Genetic correlations and genome-wide associations of cortical structure in general population samples of 22,824 adults. Nat Commun 11:4796.
49. Zhou Z, Wei D, Liu W, Chen H, Qin S, Xu P, *et al.* (2023): Gene transcriptional expression of cortical thinning during childhood and adolescence. Hum Brain Mapp 44:4040–4051.
50. Baron-Cohen S (2017): Editorial Perspective: Neurodiversity—A revolutionary concept for autism and psychiatry. J Child Psychol Psychiatry 58:744–747.
51. Tung YH, Lin HY, Chen CL, Shang CY, Yang LY, Hsu YC, *et al.* (2021): Whole brain white matter tract deviation and idiosyncrasy from normative development in autism and ADHD and unaffected siblings link with dimensions of psychopathology and cognition. Am J Psychiatry 178:730–743.
52. Geschwind DH, Levitt P (2007): Autism spectrum disorders: Developmental disconnection syndromes. Curr Opin Neurobiol 17:103–111.
53. Floris DL, Peng H, Warrier V, Lombardo MV, Pretzsch CM, Moreau C, *et al.* (2023): The link between autism and sex-related neuroanatomy, and associated cognition and gene expression. Am J Psychiatry 180:50–64.
54. Chen G, Cai Z, Taylor PA (2024): Through the lens of causal inference: Decisions and pitfalls of covariate selection. Aperture Neuro 4.
55. Velmeshev D, Schirmer L, Jung D, Haeussler M, Perez Y, Mayer S, *et al.* (2019): Single-cell genomics identifies cell type–specific molecular changes in autism. Science 364:685–689.
56. Hawrylycz MJ, Lein ES, Guillozet-Bongaarts AL, Shen EH, Ng L, Miller JA, *et al.* (2012): An anatomically comprehensive atlas of the adult human brain transcriptome. Nature 489:391–399.